UNIVERSITY OF AMSTERDAM

UvA-DARE (Digital Academic Repository)

Coherent X-ray scattering of charge order dynamics and phase separation in titanates

Shi, B.

Publication date
2017

Document Version
Other version

License
Other

Link to publication

Citation for published version (APA):
Shi, B. (2017). *Coherent X-ray scattering of charge order dynamics and phase separation in titanates*. [Thesis, fully internal, Universiteit van Amsterdam].

General rights
It is not permitted to download or to forward/distribute the text or part of it without the consent of the author(s) and/or copyright holder(s), other than for strictly personal, individual use, unless the work is under an open content license (like Creative Commons).

Disclaimer/Complaints regulations
If you believe that digital publication of certain material infringes any of your rights or (privacy) interests, please let the Library know, stating your reasons. In case of a legitimate complaint, the Library will make the material inaccessible and/or remove it from the website. Please Ask the Library: https://uba.uva.nl/en/contact, or a letter to: Library of the University of Amsterdam, Secretariat, Singel 425, 1012 WP Amsterdam, The Netherlands. You will be contacted as soon as possible.

UvA-DARE is a service provided by the library of the University of Amsterdam (https://dare.uva.nl)

Download date:28 Apr 2025

Appendix A

Diffraction geometry and crystallographic orientation

In this appendix we discuss details of the diffraction geometry. We start out by discussing the labeling of the charge ordered titanate structure in terms of cubic and orthorhombic unit cells. We then deal with the conversion of detector positions to scattering angles and from that derive the mapping of reciprocal space onto the detector. Finally we consider the possible loss of coherence due to the large scattering angle geometry.

Fig. A.1 shows the lattice of the charge ordered titanate system, with an indication of cubic and orthorhombic lattice directions. The $(011)_o$ planes form triangular lattices of titanium atoms of equal valence. During the experiments discussed in chapter 5, the $\mathbf{q}_{(100)o}$ direction was placed parallel to the θ rotation axis while the $\mathbf{q}_{(0-11)o}$ lies in the diffraction plane, as shown in panel (b).

Fig. A.2 shows the layout of the scattering experiment in real space. The $(011)_o$ surface is parallel to the vertical θ-axis, so that the reciprocal lattice vector $\mathbf{q}_{(011)o}$ (black) lies in the scattering plane (light blue). The scattering condition is fulfilled when this vector equals the difference of the incoming and outgoing wave vectors $\mathbf{k}_{in}$ and $\mathbf{k}_{out}$. The scattered light is intercepted by the CCD detector, which has its surface perpendicular to the $\mathbf{k}_{out}(011)$ wave vector. In the following we use a coordinate system in which the y axis is normal to the surface and z is along the θ rotation axis.

The corresponding reciprocal space representation of the experiment is depicted in Fig. A.3. The incoming and outgoing wave vectors $\mathbf{k}_{in}$ and $\mathbf{k}_{out}$ define the Ewald sphere and the light blue scattering vector $\mathbf{q}$ connects the two. When the (011) diffraction condition is met, the scattering vector $\mathbf{q}$ coincides with the (011) reciprocal lattice vector $\mathbf{q}_{(011)}$. Due to the disorder in the charge order structure, the (011) diffraction spot is surrounded by a cloud of diffuse scattering, represented here by a green ellipsoid.

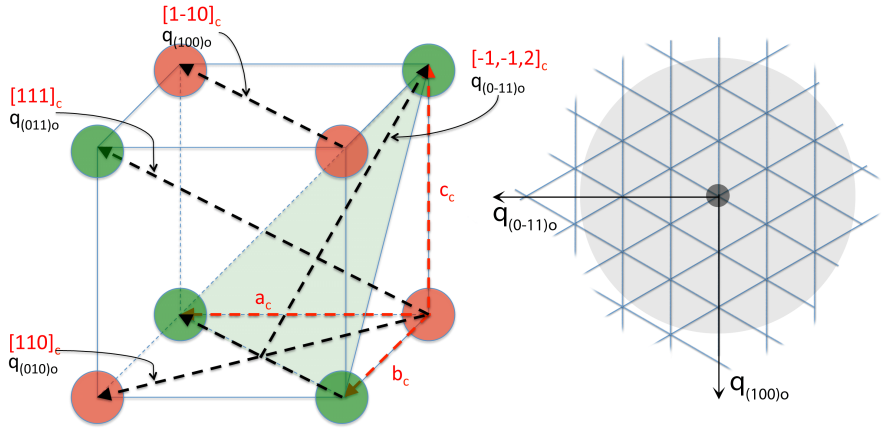

Fig. A.1 Left: the $(RCa)TiO_3$ system in the charge ordered state. The Ti^{3+} (green) and Ti^{4+} (red) ions sit in the corners of a nearly cubic unit cell. The cubic lattice vectors are indicated in red with subscript c. The **q** vectors in orthorhombic notation are denoted in black with subscript 'o'. One of the (011) planes is indicated by a green triangle. Right: a top view of the (011) plane, where $\mathbf{q}_{(011)o}$ direction is pointing out of the surface, $\mathbf{q}_{(100)o}$ is pointing down, and $\mathbf{q}_{(0-11)o}$ lies horizontally in the diffraction plane.

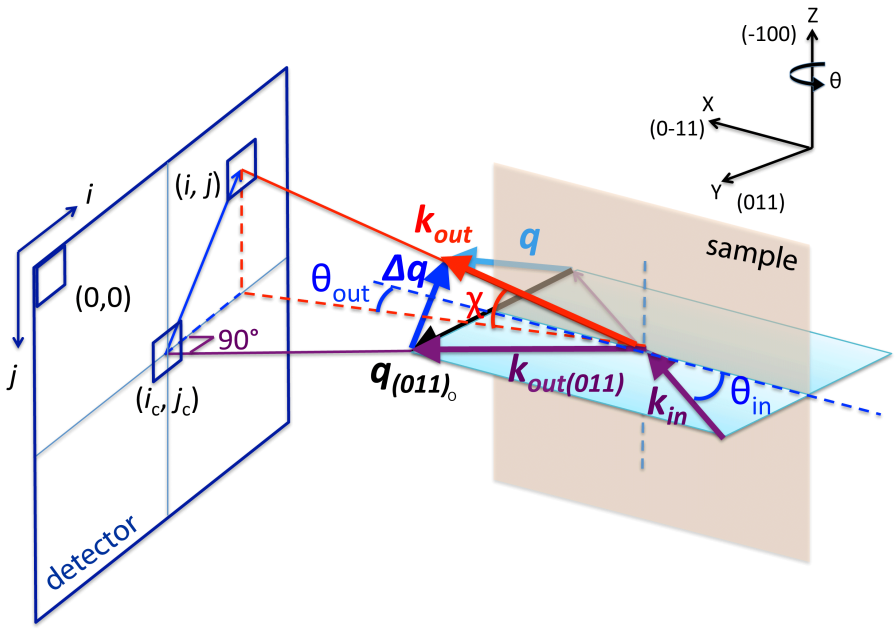

Fig. A.2 The real space representation of the scattering geometry indicating the mapping of reciprocal space to pixel positions on the CCD detector.

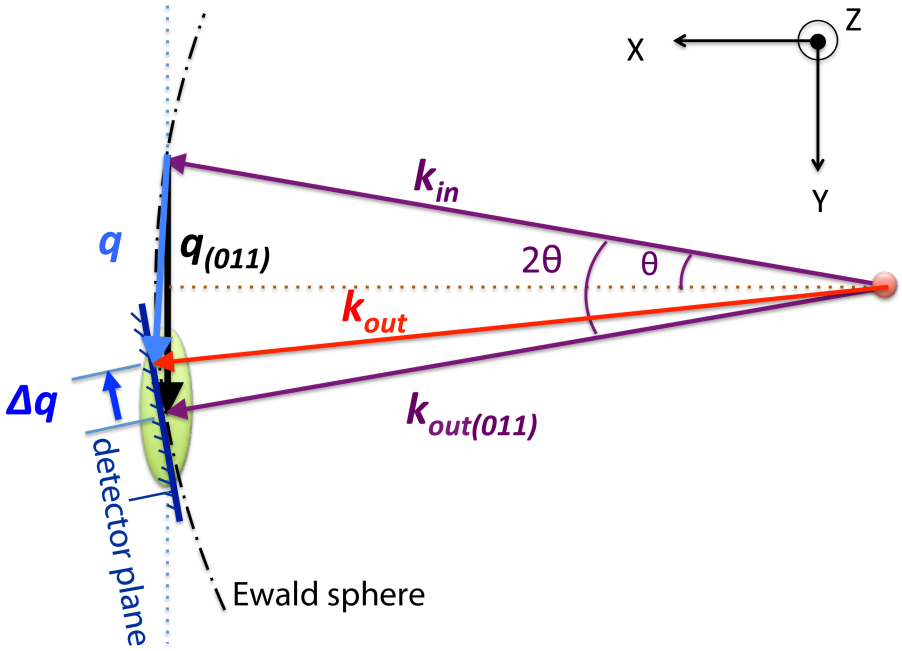

Fig. A.3 Reciprocal space representation of the scattering geometry. The green ellipse represents the diffuse scattering around the (011) reciprocal lattice point. The angles are representative of the hard X-ray experiments, $\theta = 10°$. In the soft X-ray experiments, the k_{in} vectors are much shorter and $\theta = 79°$. The angle between the detector plane and the $\mathbf{q}_{(011)}$ is equal to the diffraction angle θ.

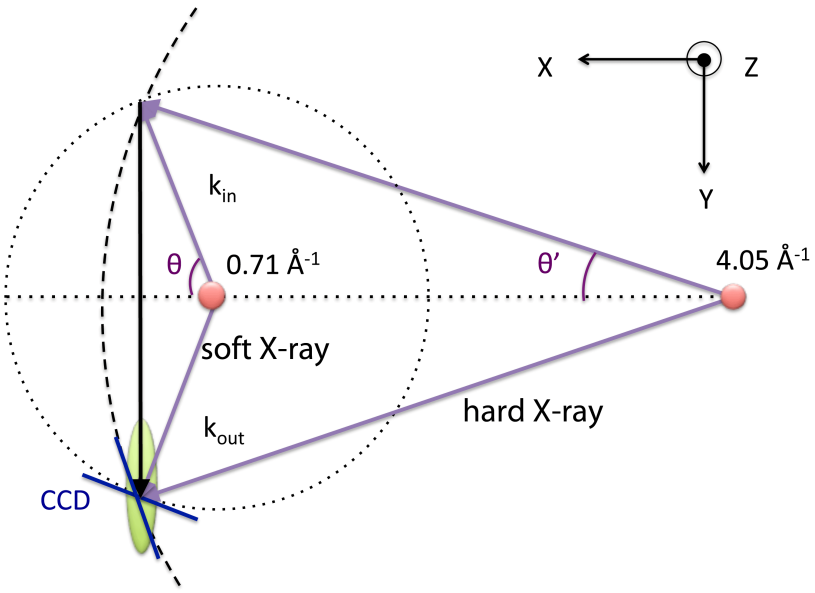

Fig. A.4 Schematic of the difference in detector cuts through the (011) reflection in reciprocal space for our soft and hard X-ray experiments. (For the latter, the red circle representing the source position in q-space should be very off the paper to the right.)

Since the detector has its surface perpendicular to k_{out}, it can be represented in reciprocal space as a tangent plane to the Ewald sphere. The alignment procedure aims to position the detector on the $\mathbf{q}_{(011)}$ reciprocal lattice vector, so that the image on the CCD detector is a cut through the diffuse scattering cloud. In that case, the center of intensity on the camera corresponds to the wave vector $\mathbf{k}_{out}$ - $\mathbf{k}_{in}$ = $\mathbf{q}_{(011)}$.

The diffuse scattering can be seen as the light that has scattered away from the (011) reflection by interaction with disorder in the crystal. The intensity on the CCD image can therefore be labeled by a relative wave vector $\mathbf{k}_{out}$ - $\mathbf{k}_{in}$ = $\mathbf{q}_{(011)}$ + $\mathbf{q}_{ij}$, where i and j are the horizontal and vertical pixel coordinates on the detector. As can be seen from Fig. A.2, $\mathbf{q}_{ij}$ can be decomposed in components $\mathbf{q}_x$, $\mathbf{q}_y$ and $\mathbf{q}_z$, where $\mathbf{q}_y$ is along the (011) surface normal and $\mathbf{q}_x$ and $\mathbf{q}_z$ are two orthogonal components in the surface plane.

Sample alignment is done by either $\theta - 2\theta$ scans, in which both angles are changed by equal increments, moving the detector along the scattering vector direction, or rocking scans, in which only θ is changed, causing the detector to rotate around the scattering vector.

Fig. A.4 compares the geometry for the hard and soft X-ray experiments. It shows that in the soft X-ray experiment the detector plane makes an angle θ=$\sim 80^\circ$ with the [011] direction, while in the hard X-ray experiments this angle, θ' is $\sim 10^\circ$.

The next task is to map the diffuse scattering on the detector in terms of the three components of $\mathbf{q}_{ij}$. To this end, one first has to map the pixel positions to the angles θ_{out} and χ that define the direction of $\mathbf{k}_{out}$, as shown in Fig. A.2. This mapping is given by

$$\theta_{out} = \theta_{in} + (i_c - i) * \delta_{pix} \tag{A.1}$$

$$\chi = (j_c - j) * \delta_{pix} \tag{A.2}$$

$$q_x = k * (cos(\theta_{out}) - cos(\theta_{in}) * cos(\chi)) \tag{A.3}$$

$$q_y = k * (sin(\theta_{out}) + sin(\theta_{in})) \tag{A.4}$$

$$q_z = k * cos(\theta_{out}) * sin(\chi) \tag{A.5}$$

$$q_T = \sqrt{{q_x}^2 + {q_z}^2} \tag{A.6}$$

$$q_{ij} = \sqrt{q_T^2 + q_y^2}. \tag{A.7}$$

Here i and j are the horizontal and vertical pixel coordinates and i_c and j_c are the coordinates of the barycenter of the scattering peak. δ_{pix} is the angular width of one pixel on the detector, determined by the pixel size and the distance between the sample and the detector.

As a final point of consideration, in large angle scattering experiments the path length differences inside the illuminated volume of the sample can become larger than the longitudinal coherence length, leading to a reduction of speckle contrast. In Fig. A.5 we show the scattering of a beam with diameter L at an angle θ. The penetration depth or extinction length H indicates the distance from the surface into the sample along the surface normal, over which the beam intensity falls to $1/e$ of the original value [117]. From the figure it can be concluded that the maximum allowable path length difference is given by $2Hsin(\theta)$. From this point of view, the experimental conditions at each of the three beamlines used in the research presented here are such that the path length difference is always shorter than the longitudinal coherence length. This means that we are always fully coherent in the longitudinal direction.

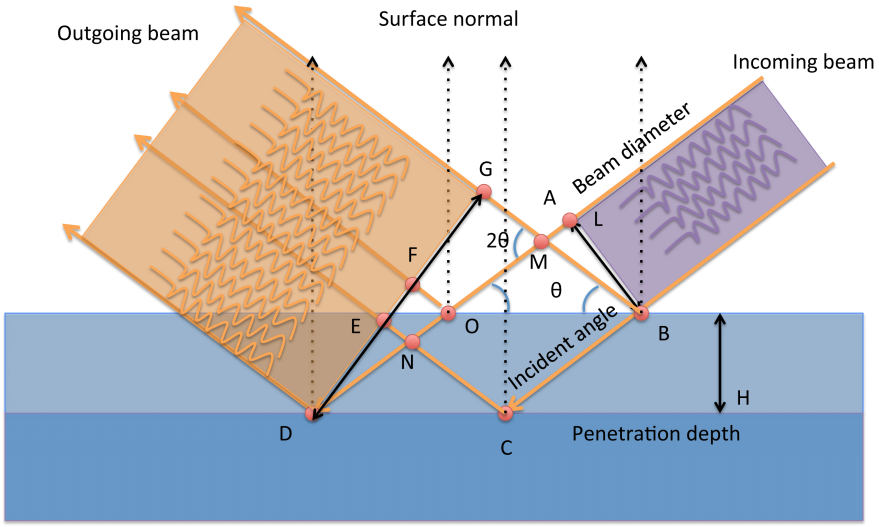

Fig. A.5 Illustration of the path length difference. L indicates the beam diameter, and H is the penetration depth. AOF and BMG are the surface reflections that have the shortest path length between flat wave fronts in the incoming and outgoing beams. AOD and BCE are the equivalent longest pathways. The path length difference is defined as the difference between the shortest and the longest path lengths, which is equal to $2Hsin(\theta)$.